The Astrophysical Journal, 585:1–11, 2003 March 1


# INHOMOGENEITIES IN THE MICROWAVE BACKGROUND RADIATION INTERPRETED WITHIN THE FRAMEWORK OF THE QUASI–STEADY STATE COSMOLOGY

J. V. Narlikar,[1] R. G. Vishwakarma,[1] Amir Hajian,[1,2] Tarun Souradeep,[1] G. Burbidge,[3] and F. Hoyle[4]

*Received 2002 February 27; accepted 2002 November 4*

## ABSTRACT

We calculate the expected angular power spectrum of the temperature fluctuations in the microwave background radiation (MBR) generated in the quasi–steady state cosmology (QSSC). The paper begins with a brief description of how the background is produced and thermalized in the QSSC. We then discuss within the framework of a simple model the likely sources of fluctuations in the background due to astrophysical and cosmological causes. Power spectrum peaks at $l \approx 6$–10, 180–220, and 600–900 are shown to be respectively related in this cosmology to curvature effects at the last minimum of the scale factor, clusters, and groups of galaxies. The effect of clusters is shown to be related to their distribution in space as indicated by a toy model of structure formation in the QSSC. We derive and parameterize the angular power spectrum using six parameters related to the sources of temperature fluctuations at three characteristic scales. We are able to obtain a satisfactory fit to the observational band power estimates of the MBR temperature fluctuation spectrum. Moreover, the values of the best-fit parameters are consistent with the range of expected values.

*Subject headings:* cosmic microwave background — cosmology: theory

## 1. INTRODUCTION

The quasi–steady state cosmology (QSSC) has been proposed by Hoyle, Burbidge, & Narlikar (1993, 1994a, 1994b, 1995) as an alternative to the standard hot big bang model. This cosmology does away with the initial singularity and does not have any cosmic epochs when the universe was very hot. The synthesis of light nuclei and the origin of the microwave background radiation (MBR) have therefore been explained by different physical processes from those invoked in the hot big bang (e.g., Hoyle, Burbidge, & Narlikar 2000; Burbidge & Hoyle 1998).

We concentrate here on the MBR, and our purpose is to explain its observed fluctuations in terms of the large-scale features of the QSSC. First, we begin with a brief description of how it is generated in this cosmology. A typical QSSC scale factor for a flat Robertson-Walker universe is given by

$$S(t) = e^{t/P}\left[1 + \eta\cos\left(\frac{2\pi\tau}{Q}\right)\right], \qquad (1)$$

where the timescales $P \approx 10^3$ Gyr $\gg Q \approx 40$–50 Gyr are considerably greater than the Hubble timescale of 10–15 Gyr of standard cosmology. The function $\tau(t)$ is very nearly like $t$, with significantly different behavior for short duration near the minima of the function $S(t)$. The parameter $\eta$ has a modulus less than unity, thus preventing the scale factor from reaching 0. Typically, $\eta \sim 0.8$–0.9. Hence, there is no spacetime singularity nor a violation of the law of conservation of matter and energy, as happens at the big bang epoch in the standard model. This is because matter in the universe is created through minibangs, explosive processes in the nuclei of existing galaxies that produce matter and an equal quantity of a negative energy scalar field $C$. Such processes take place whenever the energy of the $C$-field quantum rises above the threshold energy $m_{\rm P}c^2$, the rest-mass energy of the Planck particle that is typically created. For details of the basic physics, see Hoyle et al. (1995), and for models of the kind in equation (1), see Sachs, Narlikar, & Hoyle (1996).

While the overall energy level of the $C$-field is below this threshold, it can rise in the neighborhood of highly collapsed massive objects (objects close to becoming black holes), and these then become the sites of creation. In addition, since the overall energy density of the $C$-field scales as $S^{-4}$, the creation is facilitated near the epochs of smallest $S$. It is close to these relatively denser epochs that the creation activity is at its peak, switching itself off as the universe continues to expand in the cycle. Hence, from one cycle to another, the density of matter would have fallen by the factor $\exp(-3Q/P)$ but for the compensating creation of matter at the beginning of a new cycle at the minimum of $S$.

Thus, in the simplest model, although the universe is in a long-term steady state, it oscillates over shorter timescales, with *each cycle physically the same as the preceding one*. Each cycle has the new matter taking part in the process of formation of stars and galaxies that evolve exactly as in the previous cycle. What happens to the radiation of stars in this process? Assuming that the radiation density falls like $S^{-4}$ in each cycle, it would be depleted by the factor $\exp(-4Q/P)$ from one oscillatory minimum to the next. It is this gap that is made up by the starlight generated during the cycle, since the universe is in a steady state from one cycle to the next. Given $P$ and $Q$, and the starlight energy generated per cycle, we can estimate the radiation background at any stage of a cycle. We have shown elsewhere (Hoyle et al. 1994a, 2000) that it is this starlight thermalized by dust grains that is responsible for the MBR in the QSSC. Furthermore, the estimate of starlight generated during the typical cycle allows one to show that after thermalization, the temperature at the present epoch should be very close to 2.7 K (Burbidge & Hoyle 1998; Hoyle et al. 2000).

[1] Inter-University Centre for Astronomy and Astrophysics, Post Bag 4, Ganeshkhind, Pune 411 007, India.

[2] Institute for Advanced Studies in Basic Sciences, P.O. Box 45195-159, Zanjan 2354, Iran.

[3] Center for Astrophysics and Space Sciences 0424, University of California, San Diego, CA 92093-0424.

[4] Deceased.

In the following sections we first review the spectrum and homogeneity of the MBR in the QSSC and then describe the likely causes of inhomogeneity of the MBR. We finally compare the results with recent observations in which the fluctuations of the MBR at different angular scales have been measured.

## 2. THE SPECTRUM AND TEMPERATURE OF THE MBR

In this model it is hydrogen burning in stars in galaxies that generates the energy of the MBR, and the energy distribution of stellar radiation over different wavelengths from a typical galaxy varies through the cycle in the following way: At the minimum-$S$ epoch, new gaseous material is acquired, and new stars are formed, with the energy coming out mostly in the blue to ultraviolet from stars of masses greater than 1 $M_\odot$. However, as the cycle proceeds toward the maximum-$S$ phase after the elapse of times of the order of $\approx$25 Gyr, the massive stars burn out, leaving only the low-mass stars still shining. The typical stars thus left are the dwarfs of types $K$ to $M$, with the consequence that the radiation is then mainly in the red and the infrared. However, as the cycle proceeds toward the next minimum, these wavelengths are shortened since the universe contracts by a considerable factor.

The total energy density of starlight generated in a given cycle can be estimated from the present observations of the starlight background and by extrapolating the star-burning activity over the full cycle. Suppose that this energy density is $\epsilon$. If the background radiation energy density $u$ at the start of a cycle (when the scale factor was at its minimum value $S_m$) were $u_m$, then in the absence of any new addition to it, following the $u \propto S^{-4}$ law, this would drop to $u_m \exp(-4Q/P)$ at the end of the cycle. To maintain a steady state from one cycle to the next, therefore, the shortfall in $u_m$ is made up by $\epsilon$. Hence,

$$\epsilon = u_m\left(1 - e^{-4Q/P}\right) . \tag{2}$$

This fixes the value of $u_m$ in terms of starlight energy input. If we know the maximum redshift $z_m$ in the present cycle, we find that the present energy density of the MBR is

$$u_o = u_m(1 + z_m)^{-4} . \tag{3}$$

The details of $\epsilon$, $z_m$, $P$, and $Q$ were discussed in the papers cited above (see, for example, Hoyle et al. 2000). A present day MBR temperature of $\approx$2.7 K arises from such considerations. However, to talk of a "temperature," one must first show that the MBR has reached thermal equilibrium. We next describe briefly what must occur if this result is to be achieved.

To get an idea, we consider the typical oscillatory cycle from one minimum of the scale factor to the next. Let

$$x = \frac{S(t)}{S(t_{\min})} , \tag{4}$$

where in going from one minimum to the next we have ignored the exponential term. It is clear from this time dependence that in going from the maximum to the minimum, the scale factor drops by a factor $(1 + \eta)/(1 - \eta) \approx 12$ for $\eta \approx 0.85$. We assume as an additional parameter that the present epoch is characterized by $x = 6$.

Thus, infrared wavelengths of 1000 nm at $x = 6$ are shortened to ultraviolet wavelengths of only $\approx$160 nm at the $x = 1$ (minimum $S$) epoch. However, by this stage, the intergalactic density is increased by a factor $6^3$ as the minimum is approached, and the issue of absorption becomes important, for it is through frequent absorptions and re-emissions that the radiation background gets thermalized.

We have shown that metallic particles in the form of graphite whiskers as well as iron whiskers play a crucial role in the absorption process. As Narlikar et al. (1997) have discussed, a plausible case based on laboratory experiments and astrophysical evidence can be made for the condensation of metallic whiskers from the hot ejecta of supernovae, which are blown out into intergalactic space by the shock waves generated at the time of explosion. The extinction properties of such whiskers, typically of length $\approx$1 mm and diameter 0.01 $\mu$m, differ considerably from those of normal spherical dust. In particular, the iron whiskers at cryogenic temperatures are a dominant source of opacity in the microwave region, while carbon whiskers are more effective at the shorter UV wavelengths.

Typically, a galaxy belongs to a cluster, and we expect these whisker grains to fill up the intergalactic space within the cluster. The starlight from a galaxy in the cluster will therefore pass through such dust as it emerges out of the cluster. We therefore expect absorption and reradiation of starlight outside galaxies and also, in a larger angular scale, outside clusters. As we see below, the production of microwaves in this fashion will go on in each cycle, and the process of frequent absorption and reradiation by whiskers will eventually generate a uniform background, *except for the contribution from the latest generation of clusters*. These will stand out as inhomogeneities on the overall uniform background.

The value of the absorption coefficient $Q_{\rm abs}$ for graphite whiskers is essentially constant for all wavelengths longer than $\approx$1 $\mu$m, extending even to the long radio wavelengths, being equivalent to an absorption coefficient of $\sim 10^5$ cm$^2$ g$^{-1}$. However, it is 3 times this value for the UV radiation. Now, an intergalactic density of $\approx 10^{-34}$ g cm$^{-3}$ at $x = 6$ would rise to $\approx 2 \times 10^{-32}$ g cm$^{-3}$ at the minimum ($x = 1$) epoch. Over a cosmological distance of $10^{27}$ cm at this stage, the optical depth would be $\approx$6 for UV and $\approx$1 for wavelengths longer than 1 $\mu$m.

It is significant that this type of dust plays a role in the observed redshift–apparent magnitude relation of Type Ia supernovae. As shown by Banerjee et al. (2000), an intergalactic dust density of the above order gives a very good fit to the observations (Perlmutter et al. 1999; Riess et al. 1998). Since the results are very sensitively dependent on dust density, it cannot be fortuitous that the density for the best fit in the supernova case is of the right order to explain thermalization of the MBR. Furthermore, recent studies of the high-redshift supernova SN 1997ff ($z \simeq 1.7$) show the model to be consistent with observations within the error budget currently applicable (Vishwakarma 2002; Narlikar, Vishwakarma, & Burbidge 2002).

The great bulk of the optical radiation that becomes subject to thermalization in the contracting phase of the oscillation will have traveled a distance of the order of 10 Gpc, or even more in the case of microwaves. The radiation incident on a carbon whisker will have been in transit since the maximum-$S$ epoch of the previous cycle, and it includes all the microwave radiation existing *before* the present cycle, as

well as the starlight generated by the galaxies in the current cycle. The result is that all this radiation is well thermalized and uniform in energy density. However, the carbon whiskers themselves will be lumpily distributed on the scale of clusters of galaxies. Therefore, as the minimum of $S$ was approached at the end of the last cycle, the conversion of starlight to microwaves would have been lumpy. As the starlight is progressively absorbed, the typical grain temperature $T_g$ first rises above the MBR temperature $T_{\rm MBR}$ before dropping back to it as the grain radiates.

The effect of grains being lumpily distributed on the MBR is to cause the slight rise followed by the fall back to the MBR temperature to be lumpy too. The radiation background itself, however, does not have this lumpiness: because the total assembly of grains has a negligible heat content and is in thermal equilibrium, each grain emits as much heat as it receives. Since the emissivity of the particles does not depend on wavelength, each emits a Planck spectrum corresponding to its temperature $T_g$. Eventually, when all particles come down to the temperature $T_{\rm MBR}$, however, further absorption and re-emission bring about a strict Planck distribution at this temperature. Although, as was suggested by Narlikar, Wickramasinghe, & Edmunds (1975), thermalization can be achieved by the carbon whiskers, the presence of a small quantity of iron whiskers helps the process further. The absorption and reradiation by the whiskers at the oscillatory minimum thus generate a mixing of radiation from distances as far as $\approx 10^{29}$ cm, at the relatively low intergalactic particle densities prevalent there, in effect permitting radiation to travel freely.

## 3. THE ORIGIN OF MBR INHOMOGENEITIES

This picture suggests that the overall background will be very smooth. However, there will be some tiny fluctuations of intensity stamped on it arising from certain intrinsic inhomogeneities of the process as well as the cosmological model. We consider them in decreasing order of angular scale.

For this purpose, we propose a simple model in which the sources of inhomogeneities can be traced to the epoch of the last minimum of oscillation ($x = 1$ in our present case). This is the maximum-density epoch when the extinction by dust will be most effective. The characteristic geometrical size of the model is determined by the spacetime curvature $R$ and is of the order of $R^{-1/2}$. Any large-scale inhomogeneity of the MBR would arise over this characteristic cosmological size. This size is also featured in standard cosmology and is referred to as the "horizon size" or the "Hubble radius" (see Weinberg 1972, p. 525). For smaller sizes, we need to take note of inhomogeneity on the scale of rich clusters of galaxies, since they represent local concentrations of starlight not yet fully thermalized and redistributed. On still smaller scales, we expect to see inhomogeneities on the scale of groups of galaxies or even individual galaxies. (There should likewise be some inhomogeneity on the scale of superclusters, but it is expected to produce a weaker effect, and we ignore it in the present model.)

It is clear from the above that the issue of inhomogeneities of the MBR in the QSSC is linked with the way large-scale structures are formed in this cosmology. A structure formation scenario in the QSSC has not been developed to the level of sophistication that it has acquired in standard cosmology. A toy model by Nayeri et al. (1999) has shown, however, that the structure formation process as in the QSSC is very different from that in the standard cosmology, being essentially driven by "minicreation events" (MCEs), with gravitation playing a secondary role. Thus, the existence of galaxies and clusters at high redshifts ($z \sim 5$) is taken for granted in the QSSC picture of structure formation. The toy model of Nayeri et al. shows how clustering at various scales develops from an initial random distribution, through creation events and expansion. In a "steady state" situation, the model has to demonstrate how the physical conditions in one QSSC cycle are repeated in the next. We elaborate on this idea in § 4.

To give quantitative estimates of the above effects, we choose the same cosmological parameters that we have used to explain the redshift-magnitude relation based on Type Ia supernovae (see Banerjee et al. 2000). They are

$$H_0 = 65 \text{ km s}^{-1} \text{ Mpc}^{-1}, \quad z_{\max} = 5 \, , \qquad \Lambda_0 = -0.358 \, . \tag{5}$$

The parameters $P$ and $Q$ do not enter explicitly into the calculation, but we can typically take them to be 1000 and 50 Gyr, respectively.

The largest angular scale will arise from the size of spacetime curvature. At the present epoch, this is of the order of $(c/H_0)^{-2}$. This curvature corresponds to a linear size $c/H_0$. As we go toward the minimum–scale-factor epoch, this length scale decreases. The angle subtended at us by this length from the minimum-scale epoch can be worked out. For the parameters $P \approx 1000$ Gyr, $Q \approx 50$ Gyr, and $z_{\max} = 5$–6, we get an angular size of $\approx 10^\circ$. We therefore expect this scale to show up in the regime of relatively large angular scale fluctuations of the intensity of the MBR. The first discovery of inhomogeneity of the MBR by *COBE* (Smoot et al. 1992) was of this order.

To assess the magnitude of the fluctuations, we reproduce the arguments of Hoyle et al. (1994a). Consider the whisker grain distribution at the epoch of the last minimum of $S(t)$. The whiskers may be distributed nonuniformly to begin with, with some regions having larger whisker densities than others. Until the deviations from uniformity of radiation background become too small, they are able to push the grains down the temperature gradients to restore uniformity. Consider a fluctuation by a small factor $y$ in the average energy density $\sim 5 \times 10^{-10}$ ergs cm$^{-3}$ of the microwaves at this stage. A fluctuation of this order is able to *move* grains of density $\rho_g$ and velocity $V$ provided that $\frac{1}{2}\rho_g V^2 \simeq 5 \times 10^{-10} y$. With $\rho_g \sim 2 \times 10^{-33}$ g cm$^{-3}$ and $V \approx 0.1c$ (an adequate speed to fill a region of size $\sim 10^{26}$ cm in the available cosmological times of the order of $10^{17}$ s), we get $y \approx 2 \times 10^{-5}$, corresponding to $\Delta T/T \approx 5 \times 10^{-6}$. This is of the right order as found by *COBE*. Thus, any temperature fluctuations above this value would create temperature gradients of such magnitude as to move the grains around from high- to low-density regions and to thereby create a uniformity. Only small enough fluctuations would therefore remain intact over regions of size $\sim 10^{26}$ cm. Regions of this order are characteristic of the curvature size referred to above.

The strongest fluctuations will, however, come from rich clusters of galaxies lying in the present cycle. These denote the late additions to the background already in existence from starlight of previous cycles. Note that the light from stars belonging to galaxies in clusters of earlier generations

will already have been fully thermalized, and such clusters will not stand out as fluctuations. It is only the newer clusters at the last oscillatory minimum, with inadequate time to have been merged into the rest of the thermal background, that would produce fluctuations. A typical cluster produces the extra starlight, which on subsequent thermalization produces an additional temperature $\Delta T$ over the average background temperature $T$. Such a fluctuation will be confined to the neighborhood of the cluster. We show below how to estimate it.

Imagine a 10 Mpc size region, typically containing $\approx 10^4$ galaxies, each emitting starlight at the rate of $\approx 10^{44}$ ergs s$^{-1}$ (corresponding to an average galaxy with an absolute magnitude of $-21.4$). The flux of radiation in the form of degraded starlight across the surface of this region (assumed to be a sphere of radius 5 Mpc) is approximately $3.35 \times 10^{-4}$ ergs s$^{-1}$ cm$^{-2}$. Now, the present energy density of the MBR, $\approx 4.2 \times 10^{-13}$ ergs cm$^{-3}$, implies that by the $(1+z)^{-4}$ rule, it was $6^4$ times this value at the epoch of the last minimum of $S$. Using Stefan's law, the flux across a sphere of radius 5 Mpc for this radiation will be $c/4$ times the energy density, i.e., about 4.08 ergs s$^{-1}$ cm$^{-2}$. Comparing the excess flux due to the galaxies in this region computed above with this value, we find that there is an excess flux equal to $8.21 \times 10^{-5}$ of the average background. Equating this to $4\Delta T/T$, we find that the temperature fluctuation $\Delta T \simeq 56\,\mu$K.

Because of the inhomogeneity of the universe on the scale of clusters, the calculation cannot be made more precise, and at this stage one should look only at its order of magnitude. The fact that this calculation yields a temperature fluctuation of the order reported by the various observations is, from the point of view of the QSSC, very encouraging.

Clusters of galaxies are normally associated with a temperature decrement because of the Sunyaev-Zeldovich (SZ) effect. Indeed, observations show such effects for clusters of redshifts $\lesssim 1$. By contrast, the effect described above is predominant for clusters of large redshifts $\sim 5$, corresponding to the epoch of the last minimum of the scale factor. Thus, we expect the thermalization effect to dominate over the SZ effect for such clusters, whereas for later epochs, the former effect gets reduced, since dust extinction is much less. A more detailed study of cluster formation and evolution in the QSSC is required to decide at what stage clusters begin to acquire hot gas and when the gas temperature rises to levels at which the SZ effect becomes important. After such a study is carried out, it will be possible to estimate the average SZ decrement of temperature in any given direction by integrating over redshifts going up to the above stage.

Over and above the clusters, we expect smaller scale fluctuations on the scales of individual galaxies. The metallic whiskers are generated and ejected from inside a typical galaxy. They have escape velocities that take them well beyond the galaxy into its immediate external environment. Thus, we expect that the extra starlight generated by the galaxy will provide a slight excess of $\Delta T$ in this region after thermalization. The typical length scale of a small group of galaxies would be 1–2 Mpc.

## 4. RELATIONSHIP TO STRUCTURE FORMATION

From the above discussion, it is clear that according to the QSSC, the fluctuations of the MBR arose at relatively recent epochs (associated with the last minimum of expansion of the scale factor), and they would be related to the large-scale structure in the universe. We therefore outline briefly the current ideas on this topic in the framework of the QSSC. We consider in particular the formation and distribution of clusters of galaxies, since they turn out to have the most significant effect on the smoothness of the MBR. For details, we refer the reader to Banerjee & Narlikar (1997) and Nayeri et al. (1999).

### 4.1. *Gravitational Stability*

To begin with, it is necessary to contrast the structure formation process in the QSSC with that in standard cosmology. In standard cosmology, structure formation begins in the form of small-scale fluctuations in the spacetime metric as well as matter contents, fluctuations that are believed to be of quantum origin. These fluctuations then evolve as they grow under the effect of gravitation, with the inflationary phase playing an essential role by modifying the spectrum of inhomogeneities to the scale-invariant form. The inhomogeneities continue to grow, with gravitational clustering playing a major role. Since radiation and matter (at least the baryonic part) were strongly coupled in the early epochs, the growth of fluctuations in matter affects radiation as well. This interaction continues until the surface of last scattering, and the inhomogeneities imprinted on the radiation background at that stage get imprinted on the MBR and can be observed today.

It is essential to appreciate that the above scenario *does not occur* in the QSSC, whose past history is quite different from that of the standard cosmology. In the QSSC the quantum-gravity–dominated epoch as well as inflation did not occur, nor was there a surface of last scattering. Thus, to understand the presence of fluctuations in the MBR, one needs to look at an entirely different scenario in which the creation of matter at periodic intervals of a finitely oscillating universe having a long-term de Sitter–type expansion plays a key role.

That the gravitational force does not play the primary role in structure formation in this scenario is seen from the work of Banerjee & Narlikar (1997), wherein these authors looked at the evolution of small departures from the spacetime metric of the QSSC as well as its matter density and flow vector. Specifying the unperturbed metric by the flat Robertson-Walker line element,

$$ds^2 = dt^2 - S^2(t)\left[\left(dx^1\right)^2+\left(dx^2\right)^2+\left(dx^3\right)^2\right] , \qquad (6)$$

with $S(t)$ given by equation (1), the perturbed metric is written as

$$g_{\mu\nu} = -S^2(\eta_{\mu\nu} + h_{\mu\nu}), \quad g_{0\mu} = h_{0\mu} ,$$
$$g_{00} = 1 + h_{00} . \qquad (7)$$

Here $\eta_{\mu\nu}$ is the Minkowski metric ($\mu, \nu = 1, 2, 3$; $x^\mu$ spacelike coordinates, and $x^0 = t$) and $| h_{\mu\nu} | \ll 1$. Likewise, the density is perturbed from $\rho_0$ to $\rho_0 + \rho_1$, with $| \rho_1/\rho | \ll 1$, and the flow vector from $u_0^i = (1, 0, 0, 0)$ to $(u_0^i + u_1^i)$, with $| u_1^i | \ll 1$.

The perturbed set of field equations therefore describes the full gravitational effect on the perturbations. Banerjee & Narlikar (1997) found that in a typical oscillation, these perturbations grow to a limited extent before subsiding. These authors therefore concluded that gravitational effects can-

not play a major role in forming large-scale structure in the QSSC.

In fact, the dynamics of the QSSC require the existence of an additional force (besides gravitation) that is derived from a scalar field $C$ (Hoyle et al. 1995; Sachs et al. 1996). This scalar field is in turn related to the creation of matter. A look at the field equations of the QSSC will help understand why this field acts in such a way that gravitation does not play a key role in structure formation. These equations are

$$R_{ik} - \tfrac{1}{2} g_{ik} R + \lambda g_{ik} = -\kappa \left( T_{ik}^{\text{matter}} + T_{ik}^{C\text{-field}} \right) , \qquad (8)$$

where $T_{ik}^{\text{matter}}$ is the usual matter tensor, while $T_{ik}^{C\text{-field}}$ is given by

$$T_{ik}^{C\text{-field}} = -f \left( C_i C_k - \tfrac{1}{4} g_{ik} C^{\ell} C_{\ell} \right) . \qquad (9)$$

Both $\kappa = 8\pi G/c^4$ and $f$ are positive. Thus, the energy tensor of the $C$-field has a negative coefficient ($-f$) that makes its effect on spacetime structure repulsive, i.e., acting in direction opposite to gravity. *Note that this tensor acts even when no creation is going on.* This is why, during a typical oscillation, the normal gravitational processes of clustering are impeded.

A parallel can be cited from standard cosmology with a positive cosmological constant ($\lambda > 0$). In those models that have the $\lambda$-term sufficiently strong even in the early stages, gravitational clustering and formation of structures cannot take place. For example, with the currently favored value of $\lambda$, clustering ceased at $z \sim 1$.

However, the $C$-field intervenes in a different way through its property that it induces creation of matter. As discussed next, matter is created near collapsed massive objects (i.e., objects close to becoming black holes), and the created matter is ejected outward because of the negative stresses generated by the $C$-field. It is this creation phenomenon that holds the key to structure formation in the QSSC.

### 4.2. *Matter Creation: A Toy Model*

The field equations of the $C$-field show that at the point of creation of a particle of momentum $p_i$, the gradient of the $C$-field satisfies the condition $C_i = p_i$, ($i = 0, 1, 2, 3$). Thus, if the rest mass of the particle created is $m_0$, then (with the speed of light $c = 1$) we have at creation $C_i C^i = m_0^2$.

The use of this relation in the Schwarzschild solution near a massive object of mass $M$ shows that at a coordinate distance $r$, the magnitude of the $C$-field energy is raised to

$$C_i C^i = \frac{m^2}{1 - 2GM/c^2 r} , \qquad (10)$$

where $m^2$ is the magnitude of the energy at large distances from the massive object. Now, it may happen in general that $m < m_0$, so that no creation takes place. However, near a highly collapsed massive object with $r$ close enough to the Schwarzschild radius of the object, the creation condition is satisfied and creation can take place (Hoyle & Narlikar 1966).

The process normally begins by the creation of the $C$-field along with matter in the neighborhood of a compact massive object. The former, being propagated by the wave equation, tends to travel outward with the speed of light, leaving the created mass behind. However, as the created mass grows, its gravitational redshift begins to assert itself, and it traps the $C$-field in the vicinity of the object. As the strength of the $C$-field grows, its repulsive effect begins to manifest itself, thus making the object less and less bound and unstable. Finally, a stage may come when a part of the object is ejected from it with tremendous energy. It is thus possible for a parent compact mass to eject a bound unit outward. This unit may act as a center of creation in its own right.

We refer to such pockets of creation as minibangs or MCEs. A spherical (Schwarzschild type) compact matter distribution will lead to a spherically symmetric explosion, whereas an axisymmetric (Kerr type) distribution would lead to jetlike ejection along the symmetric axis. Because of the conservation of angular momentum of a collapsing object, it is expected that the latter situation will in general be more likely. Using this picture, Nayeri et al. (1999) proposed a toy model for structure formation and evolution, which is summarized next.

A large number of points ($N \sim 10^5$–$10^6$), each one representing an MCE, is distributed randomly over a unit cubical area. The average nearest neighbor distance for such a distribution is then $L \equiv N^{1/3}$. Now, suppose that in a typical MCE, each point generates another neighbor point at random within a distance $d = xL$ in three dimensions. Here, the number $x$ is a fraction between 0 and 1. We call $x$ the separation parameter. It denotes an ejected piece lying at a distance $\leq d$ from the parent compact object.

The sample cube is then homologously stretched by a linear factor $2^{1/3}$ to represent expansion of space. We now have the same density of points as before, i.e., $2N$ points over a volume of 2 units. From this enlarged cube, remove the periphery so as to retain only the inner unit cube. This process thus brings us back to the original state but with a different distribution of an average of $N$ points over a unit cube. This process is repeated $n$ times. Here the number of iterations $n$ plays the role of "time," as in the standard models of structure formation. The number distribution of points evolves as the "creation+expansion process" generates new points near the existing ones.

Not surprisingly, soon after, i.e., after $n = 3$–$4$ iterations of the above procedure, clusters and voids begin to emerge in the sample volume and create a "Persian carpet" type of pattern. As the experiment is repeated, voids grow in size while clusters become denser. Figure 1 illustrates the point distribution within a typical thin slice of thickness 0.001 of the cube and shows that expansion coupled with creation of matter is a natural means of generating voids and clusters.

To bring the toy model closer to the reality of the QSSC, Nayeri et al. (1999) proceeded as follows: Since the creation activity is expected to be confined largely to a narrow era around a typical oscillatory minimum, when the $C$-field is at its strongest, by considering the number density of collapsed massive objects at one oscillatory minimum of QSSC to be $f$, the number density at the next oscillatory minimum would fall to $f \exp(-3Q/P)$, that is, *if no new massive objects were added*. Thus, to restore a steady state from one cycle to the next, within each unit volume,

$$\omega f \equiv \left[ 1 - \exp\left( -\frac{3Q}{P} \right) \right] f \sim \left( \frac{3Q}{P} \right) f \qquad (11)$$

masses must be created anew. In other words, a fraction $\omega$ of the total number of massive objects must replicate themselves in the above fashion.

Notice that, unlike the old steady state theory that had new matter appearing continuously, we have here discrete

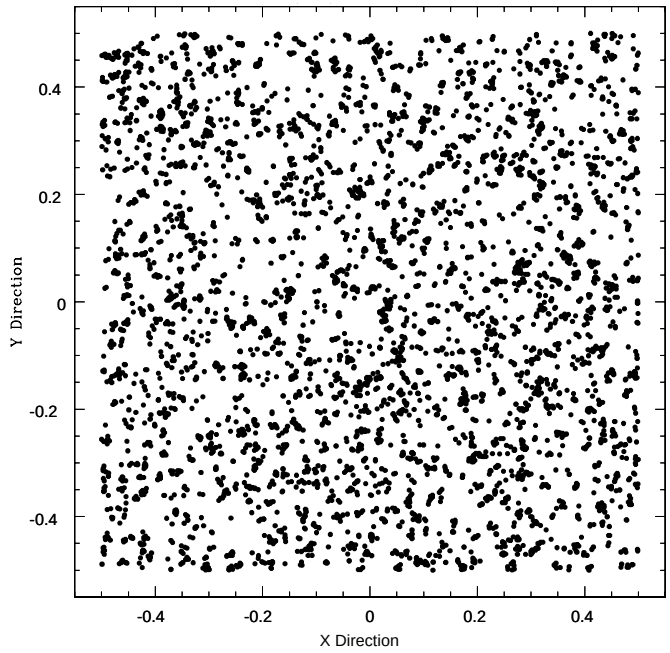


FIG. 1.—Simulation of large-scale structure in the QSSC, with $N = 1{,}000{,}000$, $x = 0.8$, $n = 10$, and $\Delta z = 0.001$, based on the creation of one generation of clusters in the vicinity of those of the previous generation, keeping aligned ejection from one generation to the next. Filaments and voids continuously develop from one generation to the next.

creation, confined to epochs of a minimum of the scale factor. The "steady state" is maintained from one cycle to the next, which is why the above fractional addition $\omega$ is required at the beginning of each cycle.

Therefore, instead of creating a new neighbor point around each and every one of the original set of $N$ points, one does so only around $\omega N$ of these points chosen randomly, where the fraction $\omega$ is as defined in equation (11). Likewise, the sample volume is homologously expanded by the factor $\exp(3Q/P)$ only, instead of by a factor of 2.

## 5. THE TWO-POINT CORRELATION FUNCTIONS

Although visual inspection of figures such as Figure 1 suggests that the toy model is proceeding along the right lines, a *quantitative* measure of the cluster-void distribution helps in comparing simulations with reality. The dimensionless autocorrelation function

$$\xi(r) = \frac{\langle [\rho(\boldsymbol{r}) - \langle\rho\rangle][\rho(\boldsymbol{r}_1 + \boldsymbol{r}) - \langle\rho\rangle]\rangle}{\langle\rho\rangle^2} , \qquad (12)$$

where $\langle\rho\rangle$ is the average density in the volume, is one convenient measure of such irregularities in the space distribution. Typically, different classes of objects cluster at different characteristic lengths. To get an idea of them, Nayeri et al. (1999) looked at the distribution of clusters of galaxies. Observationally, it is believed that the two-point correlation function for cluster distribution obeys the scaling law

$$\xi_{cc}(r) = \left(\frac{r}{r_0}\right)^{-\gamma} , \qquad (13)$$

with $\gamma \simeq 1.8$ and $r_0 = 25\ h^{-1}$ Mpc, where the Hubble constant at the present epoch is taken to be $100\ h$ km s$^{-1}$ Mpc$^{-1}$. In order to quantify the issues of formation of structures in this scenario, Nayeri et al. (1999) took the following measures:

It is known that instead of having a uniform distribution of matter on large scales, the observed universe has structures of typical sizes of a few tens of megaparsecs. These "structures" are regions of density considerably higher than the background density, with the maximum density contrast $\delta = \delta\rho(r)/\langle\rho\rangle$ going from the order of unity (in the case of clusters) to a few thousand (in the case of the galaxies).

Any process that generates structures must be able to produce to zero order entities whose density contrast is of such a magnitude, with the property that on larger and larger distance scales, the density contrast becomes less significant. This ensures that on a large enough scale, the universe is homogeneous.

Given this prescription for generating structures without gravitational dynamics, Nayeri et al. (1999) first ensured that the visual impression created by the cluster simulations did imply that as the number of iterations was increased, the number of high-density regions also increased. In the initial (totally random) configuration, one expects to find regions of high density arising only because of the Poisson noise. In the later "epochs" after a few iterations, however, one would expect to find, as in a clustering scenario, that the variation of the one-point distribution function for density $\rho/\langle\rho\rangle$ with $\langle\rho\rangle$ the average density in the volume shows a steady and significant increase in the number of high- and intermediate-density regions. This expectation was borne out, and it was also observed that the value of maximum density also increased as a function of the number of iterations, which in this experiment corresponds to "time." The density field was generated on a grid placed into the simulation volume using the algorithm of a cloud in a cell. The simulations showed the growth of structures through a rise in the density maximum as a function of the number of iterations.

A quantitative measure that was computed from these data sets was the two-point correlation function. Figure 2 shows the two-point correlation function for the case of the QSSC-based model. As time goes on, the slope of the correlation function gets closer and closer to $-1.8$. From the value of the $X$-axis intercept of the two-point correlation function, Nayeri et al. (1999) could get a rough estimate of the size of the structures in units of the size of their simulation box. From their results, they estimated that the size of the structures formed is approximately $\beta = 0.15$–$0.3$ times the box size. If one sets these values equal to the observationally accepted value of $r_0$, one can get a better physical sense of the results. If we set, for instance, $\beta = 0.3$ and $r_0 = 25\ h^{-1}$ Mpc, then the linear size of the simulation box would be $\sim 84\ h^{-1}$ Mpc. Typical cluster masses and sizes resulted from such a numerical exercise.

This may be seen as an attempt to relate the toy model to a realistic cosmological scenario. Of course, as the above exercise shows, the results can be scaled up/down by rescaling the simulation parameters and thus are independent of the "absolute" size of the box. A more detailed dynamical theory of the creation process will help relate the absolute size of clustering to the theoretical parameters.

We now examine the typical angular scales of these three types of inhomogeneities and how they are reflected in the angular power spectrum of the MBR. As far as clusters are

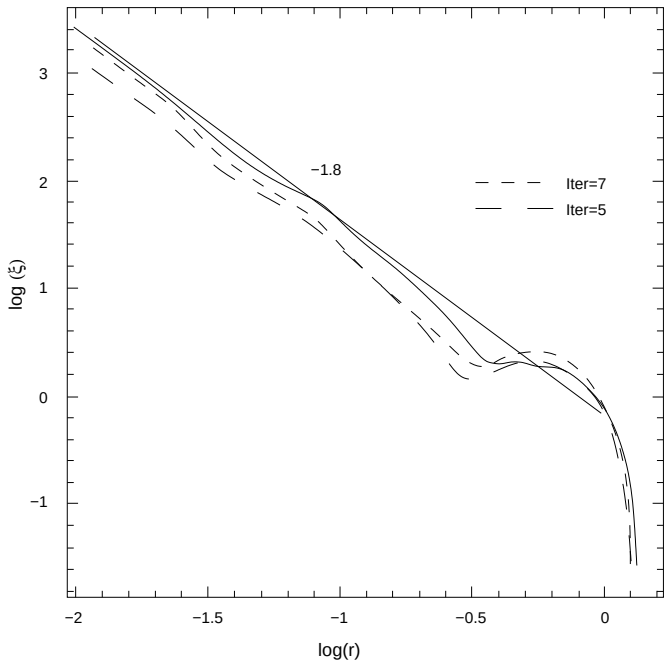


FIG. 2.—Two-point correlation function for simulations of the kind shown in Fig. 1, with a power-law–type distribution and an index approaching −1.8 after a few iterations of the process of creation. The evolution of the index toward the ideal −1.8 slope line (*solid line*) is shown as the process goes on for up to 10 generations.

concerned, we fold the above evolving two-point correlation function into our calculation.

## 6. THE ANGULAR POWER SPECTRUM OF INHOMOGENEITIES

Typically, we look at the angle subtended by a linear scale $a$ of an object located at redshift $z$ in the quasi–steady state model whose scale factor is defined in equation (1). To compute the above angle, we define the dimensionless parameters by the following formulae:

$$\Omega_0 = \frac{8\pi G\rho_0}{3H_0^2}: \text{ density parameter},$$

$$\Lambda_0 = \frac{\lambda}{3H_0^2}: \text{ cosmological constant parameter},$$

$$\Omega_{c0} = \frac{8\pi G\rho_{c0}}{3H_0^2}: \text{ creation density parameter},$$

$$K_0 = \frac{k}{H_0^2 S_0^2}: \text{ curvature parameter}. \quad (14)$$

Here $\lambda$ is the cosmological constant, which is negative in the QSSC. In the model considered by Banerjee et al. (2000) as well as here, $K_0 = 0$. The angle subtended at the observer by the above scale at redshift $z$ (see Banerjee & Narlikar 1999) is then given by

$$\alpha = \frac{H_0 a(1+z)}{c}\left(\int_1^{1+z}\frac{dy}{\sqrt{\Lambda_0 + \Omega_0 y^3 + \Omega_{c0} y^4}}\right)^{-1}. \quad (15)$$

We take $z = z_{\max} = 5$. (The maximum redshift used here is indicative only. The results do not change much, even if it were increased to 6–10.) The calculation, using the parameters of equation (5), then gives

$$\alpha = \frac{\pi a}{3600}, \quad (16)$$

where $a$ is measured in units of megaparsecs. Unless explicitly stated otherwise, angles are referred to in radians.

This then is the characteristic angle subtended by an object of linear size $a$, viewed when close to the last minimum. Assuming that this is the size of a rich cluster of galaxies, we expect that the characteristic angular sizes of the MBR inhomogeneities it generates are of this order. As we shortly show, this does translate to a peak in the angular power spectrum at a harmonic of the order of $l \approx 1/\alpha$. Therefore, we arrive at the following approximate relationship between cluster size and the harmonic it generates:

$$l \simeq \frac{3600}{\pi a}. \quad (17)$$

If we set $a \approx 2 \times$ radius of curvature at the last minimum, we expect a large angle peak at $l \approx 6$–10. The smaller angle peaks will occur at much larger values of $l$. Thus, a peak in the power spectrum of MBR anisotropy at the harmonic $l \approx 200$ as observed by the BOOMERANG and MAXIMA groups (de Bernardis et al. 2000; Hanany et al. 2000) is generated in this theory by rich clusters of diameter ≈5.5 Mpc, located at cosmological distances. Smaller peaks are expected on the scale of groups of galaxies at the higher values of $l \approx 500$–1000 and on the scale of superclusters at the lower values of $l \approx 10$–20. These latter peaks will be smaller than the cluster peak at $l \approx 200$, and thus they will be much more difficult to detect.

We next show that these expectations are borne out by detailed calculations of this effect on the angular power spectrum of the MBR. We model the above effect as follows: Imagine a typical type of inhomogeneity as a set of small disk-shaped spots, randomly distributed on a unit sphere. The spots can be either a "top-hat" or "Gaussian" type. In the former case, they have sharp boundaries, whereas in the latter case, they taper outward. We assume the former for clusters and the latter for the curvature effect and also for galaxies or groups of galaxies. This is because the clusters tend to have rather sharp boundaries, whereas in the other two cases, such sharp limits do not exist.

Let us begin with the simple case of a random distribution of infinitesimally small spots. With each direction $\hat{\boldsymbol{n}}_i$ for a typical spot center on the sky chosen randomly, we have from $N$ such spots of roughly identical temperature fluctuation $\Delta T_c$

$$\Delta T(\hat{\boldsymbol{n}}) = \sum_{i=1}^{N} \hat{a}_{n_i}\delta(\hat{\boldsymbol{n}} - \hat{\boldsymbol{n}}_i)\Delta T_c. \quad (18)$$

Here $\hat{\boldsymbol{n}}$ is a general direction on the unit sphere. If the locations of the spots in the sky are uncorrelated, we have

$$\langle \hat{a}_{n_i}\hat{a}_{n_j}\rangle = \delta_{ij}. \quad (19)$$

Writing $\Delta T$ as a function on the sphere, we expand it in a series of $Y_{lm}(\theta, \phi)$:

$$\Delta T(\hat{\boldsymbol{n}}) = \sum_{lm} a_{lm} Y_{lm}(\hat{\boldsymbol{n}}). \quad (20)$$

The expansion of $\delta(\hat{\boldsymbol{n}} - \hat{\boldsymbol{n}}_i)$ in terms of the spherical harmonic functions allows us to obtain

$$a_{lm} = \sum_{i=1}^{N} \hat{a}_{n_i} Y^*_{lm}(\hat{\boldsymbol{n}}_i)\Delta T_c \ . \tag{21}$$

The corresponding angular power spectrum is given by

$$\mathscr{C}_l \equiv \frac{l(l+1)}{2\pi}\frac{1}{(2l+1)}\sum_m \langle a^*_{lm} a_{lm}\rangle = \frac{l(l+1)}{2\pi}\frac{N}{4\pi}(\Delta T_c)^2 \ . \tag{22}$$

In the last step we use equation (19), which encodes our simplistic assumption of uncorrelated spots. We get, for large $l$, $\mathscr{C}_l \propto l^2$. This result is valid for angular scales much larger than the angular scale of the typical spot. The $l^2$ rise is a direct consequence of assuming that the locations of the spots are uncorrelated. More detailed modeling in which the correlation between the spots is included would serve to soften the $l^2$ rise. It may be an important issue when comparing our results with observations of MBR inhomogeneity on large angular scales.

However, we need to model spots of finite sizes ranging from $\approx 10^\circ$ to a few arcminutes, corresponding to the three typical inhomogeneities discussed above. For spots of finite size, assumed to be circularly symmetric with a given profile centered on the typical spot center, we have a modification of equation (18) in the form (where the delta function is replaced by a function $f$)

$$\Delta T(\hat{\boldsymbol{n}}) = \sum_{i=1}^{N} \hat{a}_n \Delta T_c f(\hat{\boldsymbol{n}} \cdot \hat{\boldsymbol{n}}_i) \ . \tag{23}$$

Using the circular symmetry of the spots, we expand

$$f(\hat{\boldsymbol{n}} \cdot \hat{\boldsymbol{n}}_i) = \sum_l \frac{(2l+1)}{4\pi} f_l P_l(\hat{\boldsymbol{n}} \cdot \hat{\boldsymbol{n}}_i) \tag{24}$$

in terms of its Legendre transform $f_l$. It is then possible to express

$$\mathscr{C}_l = \frac{l(l+1)}{2\pi}\frac{(\Delta T_c)^2}{4\pi}\sum_i \sum_j \langle \hat{a}_{n_i} \hat{a}^*_{n_j}\rangle f_l^2 P(\hat{\boldsymbol{n}}_i \cdot \hat{\boldsymbol{n}}_j) \ . \tag{25}$$

Assuming the location of the $N$ spots to be uncorrelated and randomly distributed (see eq. [19]), this gives

$$\mathscr{C}_l = \frac{l(l+1)}{2\pi}\frac{N}{4\pi}(\Delta T_c)^2 f_l^2 \ . \tag{26}$$

For a normalized Gaussian spot profile with typical (1 $\sigma$ width) angular size $\alpha$, the function $f_l$ is given by

$$f_l(\alpha) = \exp\left(-\frac{l^2\alpha^2}{2}\right) \ . \tag{27}$$

The angular power spectrum $\mathscr{C}_l \propto l^2 e^{-l^2\alpha^2}$ has a single peak at $l_p \approx \alpha^{-1}$.

For a top-hat profile, wherein the spot has a uniform temperature fluctuation across a finite disk of angular size $\alpha$, with a sharp drop-off to the background temperature outside, the function $f_l$ is given by

$$f_l(\alpha) = \frac{1}{(l+1)^2}\left[\frac{\cos\alpha P_l(\cos\alpha) - P_{l-1}(\cos\alpha)}{(2\sin^2\alpha/2)}\right] \ . \tag{28}$$

The $\mathscr{C}_l$ in this case has a series of peaks in the multipole space. The first peak in $\mathscr{C}_l$ for top-hat spots occurs at $l_p \approx \pi/2\alpha$ and has the largest amplitude. The successive peaks occur roughly at integer multiples with diminishing peak amplitude.

We therefore consider a composite model in which the inhomogeneities of the MBR arise from a superposition of random spots of three characteristic sizes corresponding to the three effects discussed above. From the order-of-magnitude estimates made earlier, we expect three peaks in the angular power spectrum at their respective $l$-ranges. To check the accuracy of this expectation, we consider a six-parameter modeling of the angular power spectrum:

$$\begin{aligned}\mathscr{C}_l = {} & A_1 l(l+1)e^{-l^2\alpha_1^2} \\ & + A_2 \frac{l}{l+1}\left[\frac{\cos\alpha_2 P_l(\cos\alpha_2) - P_{l-1}(\cos\alpha_2)}{2\sin^2\alpha_2/2}\right]^2 \\ & + A_3 l(l+1)e^{-l^2\alpha_3^2} \ ,\end{aligned} \tag{29}$$

with the parameters $A_1$, $A_2$, $A_3$, $\alpha_1$, $\alpha_2$, and $\alpha_3$ determined by obtaining the best fit with the present observations of the angular power spectrum of MBR inhomogeneities. The parameters $A_1$, $A_2$, and $A_3$ depend on the number density as well as the typical temperature fluctuation of each kind of spot. However, given $A_1$, $A_2$, and $A_3$, it is possible to compute the rms temperature fluctuation contributed by each component to the overall MBR temperature fluctuations.

If the model is successful, the values of $\alpha_1$, $\alpha_2$, and $\alpha_3$ (or the corresponding multipole value $l_p$ at which the $\mathscr{C}_l$ from each component peaks) and the rms temperature fluctuations for components would turn out to be within the range of values expected on the basis of the physics of the processes.

The analysis until now has assumed that the distribution of hot spots is uncorrelated. As described in § 5, the toy model of structure formation within QSSC does recover the observed power-law spatial correlation in the distribution of clusters. We extend the computation of the MBR anisotropy spectrum to the case in which the hot spots are correlated. We do this only for the hot spots that are linked to the clusters. Then, equation (19) is revised to

$$\langle \hat{a}_{n_i} \hat{a}^*_{n_j}\rangle = w(\theta) \ , \tag{30}$$

where $w(\theta)$ is angular correlation of clusters on the angular scale $\theta = \cos^{-1}(\hat{\boldsymbol{n}}_i \cdot \hat{\boldsymbol{n}}_j)$. The form of $\mathscr{C}_l$ in equation (26) is revised to

$$\mathscr{C}_l = \frac{AN}{8\pi^2} l(l+1) f_l^2 u_l \ , \tag{31}$$

where $w(\theta) = \sum_l (2l+1)/(4\pi) u_l P_l(\hat{\boldsymbol{n}}_i \cdot \hat{\boldsymbol{n}}_j)$. The angular correlation $w(\theta)$ can be related to the three-dimensional spatial correlation function $\xi(r)$ using the well-known Limber equation (see Peebles 1980). In particular, for a power-law correlation function $\xi(r) = (r/r_0)^{-\gamma}$, it can be shown that $w(\theta) \propto \theta^{1-\gamma}$ for the $\theta \ll 1$ limit and $1 < \gamma < 6$. In this case, $u_l \propto l^{\gamma-3}$ for $\gamma \leq 3$ (Peebles & Hauser 1974). The correlation of the hot spots due to clusters is expected to be bounded within $\gamma = 3$, the limit of uncorrelated spots, and $\gamma \sim 2$, the correlation function that the cluster distribution evolves to within the QSSC model. Consequently, we also consider an extended model with an extra parameter $\gamma$,

corresponding to an angular power spectrum

$$\mathscr{C}_l = A_1 l(l+1)e^{-l^2\alpha_1^2} + A_2 \frac{l^{\gamma-2}}{l+1}\left[\frac{\cos\alpha_2 P_l(\cos\alpha_2) - P_{l-1}(\cos\alpha_2)}{2\sin^2\alpha_2/2}\right]^2 + A_3 l(l+1)e^{-l^2\alpha_3^2}\ , \quad (32)$$

where all the other parameters are as described in equation (29).

## 7. COMPARISON WITH OBSERVATIONS

We now compare our "three-component model" with a published data compilation available at the time of writing. Figure 3 describes the error bars of the observed data that indicate the extent of scatter at present (Podariu et al. 2001). The data have been binned into 16 bins in multipole space with a mean $\Delta T_l \equiv \sqrt{\mathscr{C}_l}$ over the bin and a 1 $\sigma$ error bar (Table 2, Podariu et al. 2001). Two peaks are easily visible at $l \sim 10$ and 200, while a third peak at the much higher value of $\sim$600 is probably present. The $l$-values can be related to the physical dimensions of the sources of inhomogeneities by formula (17). For the actual fitting, we have used the above binned data.

We first discuss the case of uncorrelated spots ($\gamma = 3$). Figure 4 shows the best-fitting angular power spectrum curve $\Delta T_l$ obtained for QSSC by using a six-parameter model for the characteristic angular sizes $\alpha_i$ of the spots and the corresponding amplitudes $A_i$. For a given type of spot, the angular size can be readily related to the multipole $l_p$ at which the contribution to $\mathscr{C}_l$ peaks. The amplitudes are used to compute the rms temperature fluctuation $\Delta T_{\rm rms}$ contributed by each of the components. For the best-fit model we find $l_{p1} \simeq 27$, $l_{p2} \simeq 182$, $l_{p3} \simeq 502$, $\Delta T_{\rm rms1} \simeq 20$ $\mu$K, $\Delta T_{\rm rms2} \simeq 31$ $\mu$K, and $\Delta T_{\rm rms3} \simeq 16$ $\mu$K. For the QSSC model we have used six parameters to obtain the above fit with a minimum $\chi^2$ of 16.8. We divide the minimum $\chi^2$ value by $16 - 6 = 10$ degrees of freedom to arrive at the value of 1.68 for the reduced $\chi^2$ for our fit. This is useful for a comparison with any other model.

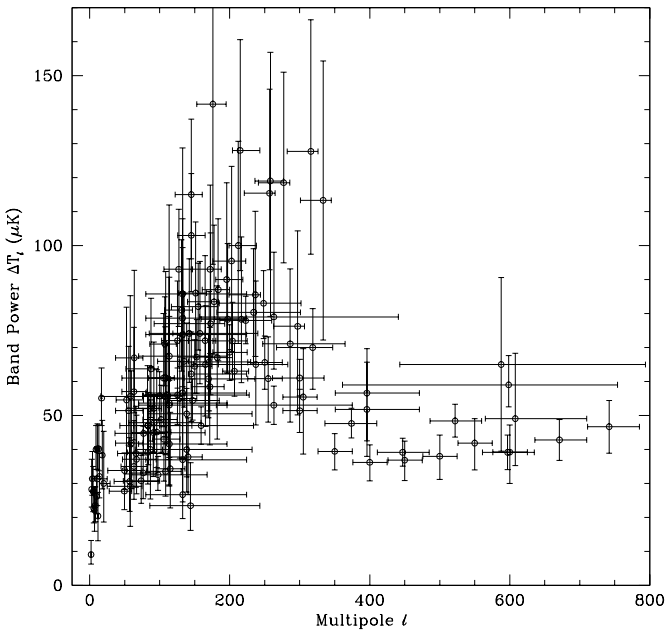


FIG. 3.—Band power spectrum of the MBR temperature inhomogeneity, measured (>2 $\sigma$ detections only) by the different experiments. The compilation of Podariu et al. (2001) has been used.

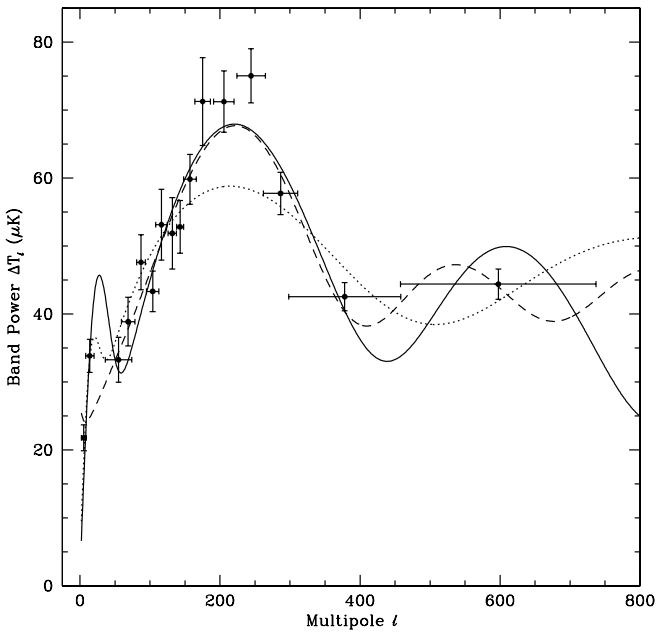


FIG. 4.—Best-fitting angular power spectrum curves in the QSSC for $\gamma = 3$ (*solid curve*) and $\gamma = 2$ (*dotted curve*), plotted and compared with the one for the favored big bang model with $\Omega_\Lambda = 0.7$ (*dashed curve*). The fitted data set is the one described in Fig. 3 and has been averaged into 16 bins in multipole space (Podariu et al. 2001).

It is encouraging to note that the parameters for the best-fit model are broadly consistent with our expectations. The value of $l_{p3} \simeq 500$ is somewhat below the expected range of 600–900. This is most likely because the largest central multipole value of the binned data set is $l \sim 600$. Since the MBR anisotropy in large multipole bands is determined and included in the binned data, we expect the best-fit values of $l_{p3}$ (and possibly, $\Delta T_{\rm rms3}$) to go up. We also note the significance of the top-hat approximation to spot profiles in clusters in our fit to the data. If we replace the top-hat profile of cluster anisotropy by a Gaussian, then we can find a best-fit model with $\chi^2 \sim 23$ with parameters $l_{p1} \simeq 25$, $l_{p2} \simeq 201$, $l_{p3} \simeq 900$, $\Delta T_{\rm rms1} \simeq 19$ $\mu$K, $\Delta T_{\rm rms2} \simeq 30$ $\mu$K, and $\Delta T_{\rm rms3} \simeq 20$ $\mu$K. Thus, the reduced $\chi^2 \sim 2.3$. The similarity in the amplitude and sizes clearly demonstrates the robustness of our model to finer details of the spot profile. The reality may lie between the two limits: the Gaussian profile and the top-hat one.

With the same binned data, we compared the anisotropy spectrum prediction of a grid of open cold dark matter (CDM) and $\Lambda$-CDM models within the standard big bang cosmology. We varied the matter density $\Omega_0$ from 0.1 to 1 in steps of 0.1, the baryon density $\Omega_b h^2$ from 0.005 to 0.03 in steps of 0.004, where $h$ is the Hubble constant in units of 100 km s$^{-1}$ Mpc$^{-1}$, and the age of the model $t_0$ from 10 to 20 Gyr in steps of 2 Gyr (Sugiyama 1995). For each value of $\Omega_0$ we considered an open model and one in which a compensating $\Omega_\Lambda$ was added to get a flat model. For the same binned data set, we found the minimum value of $\chi^2 = 23$ for the flat-universe model with $\Omega_0 = 0.7$ ($\Omega_\Lambda = 0.3$),

$\Omega_b h^2 = 0.021$, and $t_0 = 14$ Gyr ($h = 0.52$). Recent MBR inhomogeneity data, when combined with high-redshift supernova data that support nonzero $\Omega_\Lambda$ and constraints on $\Omega_0$ from large-scale structure observations, favor flat cosmological models with higher values of $\Omega_\Lambda$. In our analysis, these models have higher, but comparable, $\chi^2$ values; e.g., for $\Omega_b h^2 = 0.021$ and $t_0 = 14$ Gyr, the models with $\Omega_\Lambda = 0.6$ ($h = 0.62$) and $\Omega_\Lambda = 0.7$ ($h = 0.67$) have $\chi^2 = 24$ and 25, respectively. For comparison, the corresponding curve for the favored big bang model ($\Omega_\Lambda = 0.7$) is also shown in Figure 2.

Next we incorporate the correlation in the spots arising from clusters corresponding to spatial correlation in the distribution of clusters. In the absence of a detailed modeling of MBR anisotropy arising from clusters, we admit the entire range of $3 \geq \gamma \geq 1.8$. For $\gamma \sim 2$, we find the best-fit values $l_{p1} \simeq 18$, $l_{p2} \simeq 230$, $l_{p3} \simeq 977$, $\Delta T_{\rm rms1} \simeq 13$ $\mu$K, $\Delta T_{\rm rms2} \simeq 32$ $\mu$K, and $\Delta T_{\rm rms3} \simeq 23$ $\mu$K. For these best-fit parameters, $\chi^2 \simeq 39$. As seen in Figure 4, most of the discrepancy arises at the observed peak around $l \sim 200$, particularly from the 13th point, whose contribution to $\chi^2$ alone is $\approx$37%. This point also does not fit the standard big bang models and seems to be a general outlier. With $\gamma = 2$, the second peak in our model is broad and cannot fit the high amplitude of the peak observed in the binned compilation. At present, this may not be a significant problem for our model, even with $\gamma = 2$. As $\gamma$ is increased to 3, the fit improves rapidly. We are not in a position to fix a value of $\gamma$ that would be appropriate for the clusters at $z \sim 5$ within QSSC. On the observational front, the amplitude at the peak needs to be well established by an experiment such as the *Microwave Anisotropy Probe* (*MAP*) that covers both the low-$l$ and high-$l$ parts with good $l$-space resolution. The plot of the individual band power estimates in Figure 3 shows considerable dispersion in the central value of band power estimates, and some of discrepancies are attributed to calibration uncertainty.

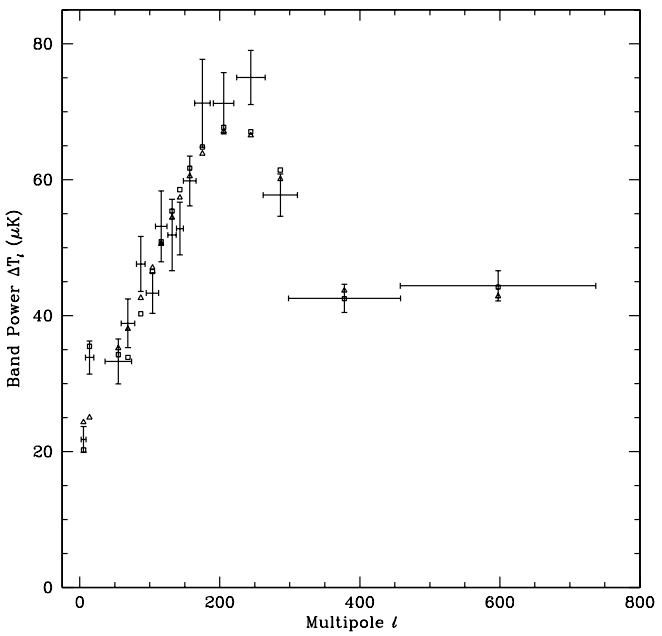


FIG. 5.—Predicted band power $\Delta T_l$ values ($\sqrt{\mathscr{C}_l}$ averaged over the 16 multipole bins), computed for the best-fitting $\gamma = 3$ QSSC model (*squares*) and the favored big bang model (*triangles*) and compared with the observed binned values.

In Figure 5 we compare the band power values $\sqrt{\mathscr{C}_l}$, averaged within the 16 multipole bins for the best-fit QSSC and the favored big bang ($\Omega_\Lambda = 0.7$) models, with the binned values of the observed MBR inhomogeneity data. Within QSSC, the unclustered hot spots allow for a very good fit to the MBR data up to l600. The peak around $l \sim 200$ in the present data is best fitted by uncorrelated spots, and the fit around the peak is adversely affected as the correlation between the spots is increased. We also find that the details of the spot profile do not affect the fit significantly.

## 8. CONCLUDING REMARKS

In the QSSC the MBR arises from the matter in galaxies, and this is quite different from its origin in the hot big bang cosmology. For example, the major peak (at $l \approx 200$) in the MBR in the framework of the QSSC is explained in terms of rich clusters of galaxies, whereas in the hot big bang cosmology, it is the Doppler peak associated with acoustic oscillations of the photon-baryon fluid. The QSSC interpretation links the inhomogeneities of the radiation field to those of the matter field, visible matter in the form of clusters of galaxies. Indeed, one can argue that in the QSSC interpretation, the observations of MBR inhomogeneities provide us with a direct diagnostic of the structural hierarchy in the universe. For example, the pattern of patchiness around $l \sim 200$ depends on the cluster-cluster correlation function. However, we must use the clusters at large redshifts ($\approx$5) for accurately estimating the magnitude of the effect. In this paper we account for the effect of the cluster-cluster correlation function based on earlier published results obtained using toy-model structure formation within QSSC. We hope to carry out such an analysis when more complete data on the cluster distributions are available, going back to epochs of high redshift, and the theory of structure formation and evolution in the QSSC makes further progress.

In addition, from Figure 4 we see that peaks occur at different locations for $l > 500$ for the most favored big bang model and the best-fitting QSSC model. Future observations at high values of $l$ from *MAP*, *Planck*, and other experiments may help distinguish between the two cosmologies.

In the end, perhaps it is best to stress the attitudinal difference between the two cosmologies. In the big bang cosmology, the inferences are related to the postulated initial conditions, prevailing well beyond the range of direct observations (at redshifts $\gtrsim$1000). In the QSSC, the attempt is to relate the patchiness of structure (at redshifts $\approx$5), which may be observable one day, to the patchiness of the MBR. These latter studies admittedly do not give predictions as sharp as those given by the former, but they may perhaps claim to be less speculative.

J. V. N. and R. G. V. acknowledge grants from the Department of Atomic Energy for support of a Homi Bhabha Distinguished Professorship for the former and an associated postdoctoral fellowship for the latter. G. B. wishes to acknowledge the hospitality given to him during his visits to IUCAA in 2001–2002. A. H. thanks IUCAA for supporting him as a project student for 6 months.

REFERENCES

Banerjee, S. K., & Narlikar, J. V. 1997, ApJ, 487, 69
———. 1999, MNRAS, 307, 73
Banerjee, S. K., Narlikar, J. V., Wickramasinghe, N. C., Hoyle, F., & Burbidge, G. 2000, AJ, 119, 2583
Burbidge, G., & Hoyle, F. 1998, ApJ, 509, L1
de Bernardis, P., et al. 2000, Nature, 404, 955
Hanany, S., et al. 2000, ApJ, 545, L5
Hoyle, F., Burbidge, G., & Narlikar, J. V. 1993, ApJ, 410, 437
———. 1994a, MNRAS, 267, 1007
———. 1994b, A&A, 289, 729
———. 1995, Proc. R. Soc. London A, 448, 191
———. 2000, A Different Approach to Cosmology (Cambridge: Cambridge Univ. Press)
Hoyle, F., & Narlikar, J. V. 1966, Proc. R. Soc. London A, 290, 143
Narlikar, J. V., Vishwakarma, R. G., & Burbidge, G. 2002, PASP, 114, 1092
Narlikar, J. V., Wickramasinghe, N. C., & Edmunds, M. G. 1975, in Far Infrared Astronomy, ed. M. Rowan-Robinson (New York: Pergamon), 131
Narlikar, J. V., Wickramasinghe, N. C., Sachs, R., & Hoyle, F. 1997, Intl. J. Mod. Phys. D, 6, 125
Nayeri, A., Engineer, S., Narlikar, J. V., & Hoyle, F. 1999, ApJ, 525, 10
Peebles, P. J. E. 1980, The Large-Scale Structure of the Universe (Princeton: Princeton Univ. Press)
Peebles, P. J. E., & Hauser, M. G. 1974, ApJS, 28, 19
Perlmutter, S., et al. 1999, ApJ, 517, 565
Podariu, S., Souradeep, T., Gott, J. R., III, Ratra, B., & Vogeley, M. S. 2001, ApJ, 559, 9
Riess, A., et al. 1998, AJ, 116, 1009
Sachs, R., Narlikar, J. V., & Hoyle, F. 1996, A&A, 313, 703
Smoot, G., et al. 1992, ApJ, 396, L1
Sugiyama, N. 1995, ApJS, 100, 281
Vishwakarma, R. G. 2002, MNRAS, 331, 776
Weinberg, S. 1972, Gravitation and Cosmology (New York: Wiley)